Results in Physics 8 (2018) 104–113

Contents lists available at ScienceDirect

Results in Physics

journal homepage: www.journals.elsevier.com/results-in-physics

Exact Riemann solutions of the Ripa model for flat and non-flat bottom topographies

Asad Rehman [a], Ishtiaq Ali [a], Shamsul Qamar [a,b,*]

[a] Department of Mathematics, COMSATS Institute of Information Technology, Park Road Chak Shahzad, Islamabad, Pakistan
[b] Max Planck Institute for Dynamics of Complex Technical Systems, Sandtorstrasse 1, 39106 Magdeburg, Germany

ARTICLE INFO

Article history:
Received 6 November 2017
Received in revised form 22 November 2017
Accepted 23 November 2017

Keywords:
Ripa system
Riemaan solution
Stationary shock wave
Rarefaction wave
Shock wave

ABSTRACT

This article is concerned with the derivation of exact Riemann solutions for Ripa model considering flat and non-flat bottom topographies. The Ripa model is a system of shallow water equations accounting for horizontal temperature gradients. In the case of non-flat bottom topography, the mass, momentum and energy conservation principles are utilized to relate the left and right states across the step-type bottom topography. The resulting system of algebraic equations is solved iteratively. Different numerical case studies of physical interest are considered. The solutions obtained from developed exact Riemann solvers are compared with the approximate solutions of central upwind scheme.

Introduction

The shallow water equations are used to simulate a large class of physical phenomena, such as currents in estuaries, bore propagation, and flood waves in surges and tsunamis. The Ripa model contains the shallow water equations and the terms accounting for horizontal temperature gradients. The Ripa model was introduced in [16,17,4] to analyze the behavior of ocean currents. The model equations form a set of nonlinear hyperbolic equations and were derived by taking into account multi-layered models and in each layer the velocity field, density and horizontal pressure gradient are vertically integrated. The presence of horizontal pressure gradients which are dependent on temperature cause the variations in fluid density within each layer. Recently, different numerical schemes were introduced to solve the Ripa model, see for instance [5,3,9,18].

The goal of this article is to derive exact Riemann solutions for the Ripa model incorporating both flat and non-flat bottom topographies. In this work, a particular shaped non-flat bottom is considered which is a step-type bottom having a fixed position of the step at which the flow variables are initially discontinuous. The knowledge about exact Riemann solution is helpful to assess and develop numerical schemes and provides a reference solution for checking their performance. As the nature of the Ripa system is hyperbolic, it admits discontinuous solutions in addition to smooth solutions. The exact Riemann solution of Ripa model with flat bottom only consists of elementary waves, such as rarefaction, shock, and contact discontinuity. For further study about elementary waves see [20,14].

The Ripa model with non-flat bottom topography is not expressible in conservative form because the presence of source term, which accounts for bottom variation, prevents the model from being conservative. This differential source term introduces several difficulties in solving the model equations analytically or numerically and conventional methods produce invalid results. In recent years, different numerical solution techniques have been introduced for better approximation of the differential source term in shallow water equations with non-flat bottom topographies [12,10,6,7,21,19]. Meanwhile the exact Riemann solvers are also introduced to handle the particular type of bottom topographies efficiently, for example see [1,2,11,8] and references therein. However, this serious issue still open for further investigation.

In present work,the Rankine-Hugoniot conditions are derived in the neighborhood of bottom discontinuity by using the principles of conservation of mass, momentum and energy. In this case, a new wave arises along the other elementary waves, which we call the stationary shock wave which is located at the step-type bottom. At the end, the system of two algebraic equations is solved for two unknowns. Once this system of algebraic equations is

* Corresponding author at: Department of Mathematics, COMSATS Institute of Information Technology, Park Road Chak Shahzad, Islamabad, Pakistan.
E-mail address: shamsul.qamar@comsats.edu.pk (S. Qamar).

https://doi.org/10.1016/j.rinp.2017.11.031
2211-3797/

solved, the remaining solution procedure is analogous to the case of flat-bottom topography.

The rest of article is organized as follows. In Section "The one-dimensional Ripa system for flat bottom", the exact Riemann solution of the Ripa system with flat bottom topography is constructed. In Section "One dimensional Ripa system with non-flat bottom", the Rankine-Hugoniot jump conditions are derived by using the conservation laws of mass, momentum and energy. These conditions are utilized to construct the exact Riemann solution of the Ripa system for non-flat bottom topography. In Section "Solution procedure", we summarize the solution procedures of Ripa model for flat and non-flat bottom topographies. In Section "Numerical tests", the solutions of developed exact Riemann are assessed by comparing them with the results of central upwind scheme, see [15]. Finally, conclusion are drawn in Section "Conclusions".

The one-dimensional Ripa system for flat bottom

The one-dimensional Ripa system with flat bottom topography has the following form [3]

$$\begin{aligned} &\partial_t h + \partial_x(hu) = 0,\\ &\partial_t hu + \partial_x\left(hu^2 + \frac{gh^2\theta}{2}\right) = 0,\\ &\partial_t h\theta + \partial_x(hu\theta) = 0. \end{aligned} \tag{1}$$

Here, h is free surface elevation, g is the acceleration due to gravity, u is the x-component of velocity, and $\theta > 0$ is the temperature of liquid. In compact form, the system in Eq. (1) can be rewritten as

$$\frac{\partial w_i}{\partial t} + \frac{\partial f_i}{\partial x} = 0, \quad i = 1,2,3, \tag{2}$$

where $w_1 \overset{\text{def}}{=} h$, $w_2 \overset{\text{def}}{=} hu$, $w_3 \overset{\text{def}}{=} h\theta$, and the fluxes are given as

$$f_1 \overset{\text{def}}{=} w_2, \quad f_2 \overset{\text{def}}{=} \frac{(w_2)^2}{w_1} + \frac{g}{2}(w_1)(w_3), \quad f_3 \overset{\text{def}}{=} \frac{(w_2)(w_3)}{w_1}. \tag{3}$$

Eigen-structure of the Ripa system for flat bottom

The quasi-linear form of the Ripa system is given as

$$\partial_t \mathbf{w} + A(\mathbf{w})\partial_x(\mathbf{w}) = 0, \tag{4}$$

where $\mathbf{w} = (w_1, w_2, w_3)^T$, and $A(\mathbf{w})$ is a Jacobian matrix of the form

$$A(\mathbf{w}) = \begin{pmatrix} 0 & 1 & 0\\ -\frac{w_2^2}{w_1^2} + \frac{gw_3}{2} & 2\frac{w_2}{w_1} & \frac{gw_1}{2}\\ -\frac{w_2w_3}{w_1^2} & \frac{w_3}{w_1} & \frac{w_2}{w_1} \end{pmatrix} = \begin{pmatrix} 0 & 1 & 0\\ -u^2 + \frac{gh\theta}{2} & 2u & \frac{gh}{2}\\ -u\theta & \theta & u \end{pmatrix}. \tag{5}$$

The eigenvalues of the matrix A are given as

$$\lambda_1 = u - a, \quad \lambda_2 = u, \quad \lambda_3 = u + a, \tag{6}$$

where $a = \sqrt{gh\theta}$ and $\lambda_1 < \lambda_2 < \lambda_3$. Thus, the given system is strictly hyperbolic. The corresponding eigenvectors are expressed as

$$\mathbf{r}_1 = \begin{pmatrix} 1\\ u-a\\ \theta \end{pmatrix}, \quad \mathbf{r}_2 = \begin{pmatrix} 1\\ u\\ -\theta \end{pmatrix}, \quad \mathbf{r}_3 = \begin{pmatrix} 1\\ u+a\\ \theta \end{pmatrix}. \tag{7}$$

Riemann solution of the Ripa system for flat Bottom

In this case, the bottom function $B(x)$ is assumed constant. The structure of Riemann solution consists of three waves, one for each eigenvalue λ_i, $i = 1,2,3$. The left most wave is either a shock wave or a rarefaction wave. Similarly, the right most wave is either a shock wave or a rarefaction wave depending on the given initial data. The third central wave is called a contact wave which always lies between the other two waves. These three waves form four different regions which are schematically depicted in Fig. 1, such as $w_L(h_L, u_L, \theta_L)$-left initial state, $w_R(h_R, u_R, \theta_R)$-right initial state, $w_{L*}(h_{L*}, u_{L*}, \theta_{L*})$-an unknown left state to the contact wave, and $w_{R*}(h_{R*}, u_{R*}, \theta_{R*})$-an unknown right state to the contact wave. In the following subsections, the above-mentioned three types of waves are further elaborated and their relations are derived.

Rarefaction waves

Rarefaction waves are continuous waves in a genuinely nonlinear 1- and 3-characteristic fields. These waves must satisfy the Riemann invariant condition

$$\frac{dw_1}{r_1^i} = \frac{dw_2}{r_2^i} = \frac{dw_3}{r_3^i},$$

where superscript i denotes the ith component of a corresponding eigenvector. We consider 1- and 3-waves as rarefaction waves. By using the Riemann invariant equalities, we obtain

$$u - 2\sqrt{gh\theta} = \text{constant across } \lambda_1 = u - a, \tag{8}$$

$$u + 2\sqrt{gh\theta} = \text{constant across } \lambda_2 = u + a, \tag{9}$$

and

$$\theta = \text{constant}. \tag{10}$$

The last equation implies that across the rarefaction wave the temperature θ remains constant. If the rarefaction wave lies on the left hand side, the left known state $\mathbf{w}_L$ is connected to the unknown state $\mathbf{w}_{L*}$ through the relation (9) as

$$u_L + 2\sqrt{gh_L\theta_L} = u_{L*} + 2\sqrt{gh_{L*}\theta_{L*}}. \tag{11}$$

According to Eq. (10), $\theta_L = \theta_{L*}$. Thus, Eq. (11) becomes

$$u_{L*} = u_L + 2\sqrt{\theta_L}\left(\sqrt{gh_L} - \sqrt{gh_{L*}}\right). \tag{12}$$

Similarly, for the right rarefaction wave, the above expression modifies to

$$u_{R*} = u_R - 2\sqrt{\theta_R}\left(\sqrt{gh_R} - \sqrt{gh_{R*}}\right). \tag{13}$$

The rarefaction wave has a fan-type shape bounded by two curves, called as tail and head. When the wave is moving to left the head is $u_L - a_L$ and the tail is $u_{L*} - a_{L*}$. At the fan area, the velocity of all particles between the head and tail obey the expression:

$$\frac{(x - x_o)}{t} = u_{L*} - a_{L*}. \tag{14}$$

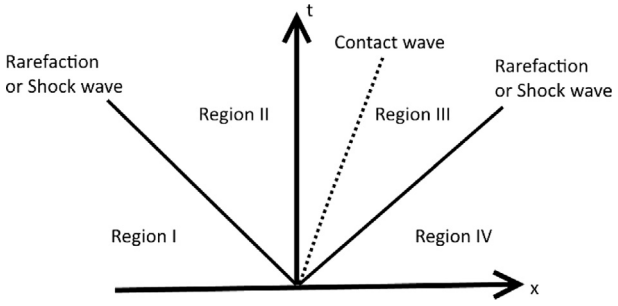

Fig. 1. Schematic diagram of four solution regions in the case of constant bottom topography.

Here x_o is the position where the flow variables are initially discontinuous. By using Eqs. (11) and (14), we can derive relations for the velocity and free-surface elevation in the fan-type area as expressed below:

$$u_{Lm*} = \frac{1}{3}\left[u_L + 2\left(a_L + \frac{(x-x_o)}{t}\right)\right], \tag{15}$$

$$h_{Lm*} = \frac{1}{9g\theta}\left[u_L + 2a_L - \frac{(x-x_o)}{t}\right]^2, \tag{16}$$

where $Lm*$ denotes the left intermediate state in the fan-type area. Similarly we can derive relations for the velocity and free-surface elevation in a fan-type area if the right wave is a rarefaction wave. Thus, we get

$$u_{Rm*} = \frac{1}{3}\left[u_R - 2a_R + 2\frac{(x-x_o)}{t}\right], \tag{17}$$

$$h_{Rm*} = \frac{1}{9g\theta}\left[-u_R + 2a_R + \frac{(x-x_o)}{t}\right]^2, \tag{18}$$

where $Rm*$ denotes the right intermediate state in the fan-type area.

Shock waves

Shock waves are discontinuous waves in a genuinely nonlinear 1- and 3-characteristic fields. Similar to the rarefaction wave, the shock can also move to either left or to the right. Shocks require the use of Rankine-Hugoniot jump conditions

$$S(\mathbf{w}_L - \mathbf{w}_R) = \mathbf{f}(\mathbf{w}_L) - \mathbf{f}(\mathbf{w}_R), \tag{19}$$

where S denotes the shock speed, $\mathbf{w}$ is the vector of conserved variables, and $\mathbf{f}(\mathbf{w})$ is the vector of fluxes. These conditions are expressed as

$$\begin{aligned} &-S[h] + [hu] = 0,\\ &-S[hu] + [hu^2] + [\tfrac{g}{2}h^2\theta] = 0,\\ &-S[h\theta] + [h\theta u] = 0, \end{aligned} \tag{20}$$

where $[\cdot]$ denotes a jump across the discontinuity. More precisely, Eq. (20) is rewritten as

$$\begin{aligned} &S(h_L - h_R) = (h_L u_L h_R u_R),\\ &S(h_L u_L - h_L u_R) = (h_L u_L^2 - h_R u_R^2) + \left(\tfrac{g}{2}h_L^2\theta_L - \tfrac{g}{2}h_R^2\theta_R\right),\\ &S(h_L\theta_L - h_R\theta_R) = (h_L\theta_L u_L - h_R\theta_R u_R). \end{aligned} \tag{21}$$

It is convenient to transform the coordinates to a new frame of reference so that shock speed is zero in the new frame of reference. During transformation, only velocities are changed to new relative velocities $\hat{u}_L$ and $\hat{u}_R$ as defined below:

$$\hat{u}_L = u_L - S, \quad \hat{u}_R = u_R - S. \tag{22}$$

Now, Eq. (21) becomes

$$h_L\hat{u}_L = h_R\hat{u}_R, \tag{23}$$

$$h_L\hat{u}_L^2 + \frac{g}{2}h_L^2\theta_L = h_R\hat{u}_R^2 + \frac{g}{2}h_R^2\theta_R, \tag{24}$$

$$h_L\theta_L\hat{u}_L = h_R\theta_R\hat{u}_R. \tag{25}$$

First we consider the right wave is the shock wave, so by using Eq. (23) the mass flux is defined as

$$h_L\hat{u}_L = h_R\hat{u}_R = -M. \tag{26}$$

By using Eqs. (24) and (26), we get the following relation

$$M^2 = \frac{g}{2}\left(h_L h_R \frac{(h_R^2\theta_R - h_L^2\theta_L)}{h_R - h_L}\right). \tag{27}$$

From Eq. (21), we can easily derive a relation for the temperature across the shock wave:

$$\theta = \text{constant}. \tag{28}$$

Assuming the right wave as a shock wave, we can connect the initial right state $\mathbf{w}_R$ to the unknown state $\mathbf{w}_{R*}$ by using Eq. (21):

$$u_{R*} = u_R + (h_{R*} - h_R)\sqrt{\frac{g}{2}\frac{(h_R\theta_R + h_{R*}\theta_{R*})}{h_R h_{R*}}}, \tag{29}$$

or by using Eq. (28), which implies that $\theta_R = \theta_{R*}$, Eq. (29) becomes

$$u_{R*} = u_R + (h_{R*} - h_R)\sqrt{\frac{g\theta_R}{2}\frac{(h_R + h_{R*})}{h_R h_{R*}}}. \tag{30}$$

Now, we obtain a relation for the speed of right shock by using Eqs. (26) and (27).

$$S = u_{R*} + \frac{M}{\varphi_{R*}}. \tag{31}$$

Similarly, we can derive relations for velocity and shock speed if the left wave is a shock wave, i.e.

$$u_{L*} = u_L - (h_{L*} - h_L)\sqrt{\frac{g\theta_L}{2}\frac{(h_L + h_{L*})}{h_L h_{L*}}}, \tag{32}$$

and

$$S = u_{L*} - \frac{M}{\varphi_{L*}}. \tag{33}$$

Contact waves

The contact wave marks the boundary at which two fluids of different densities are in contact with each other and it is associated with linearly degenerate characteristic field. By using the Riemann invariant condition

$$\frac{d(h)}{1} = \frac{d(hu)}{u} = \frac{d(h\theta)}{-\theta},$$

we obtain $u =$ constant and $h^2\theta =$constant across the contact wave discontinuity. To relate the states across the contact discontinuity, we use the Rankine-Hugoniot conditions which are given as

$$S_c(h_{L*} - h_{R*}) = h_{L*}u_{L*} - h_{R*}u_{R*}, \tag{34}$$

$$S_c(h_{L*}u_{L*} - h_{L*}u_{R*}) = h_{L*}u_{L*}^2 - h_{R*}u_{R*}^2 + \frac{g}{2}h_{L*}^2\theta_{L*} - \frac{g}{2}h_{R*}^2\theta_{R*}, \tag{35}$$

$$S_c(h_{L*}\theta_{L*} - h_{R*}\theta_{R*}) = h_{L*}\theta_{L*}u_{L*} - h_{R*}\theta_{R*}u_{R*}, \tag{36}$$

where S_c is the propagating speed of contact discontinuity. Moreover, the speed of contact discontinuity is $\lambda_2 = u$ and, therefore, $S_c = u$. The Eq. (34) implies that $u_{L*} = u_{R*} = S_c$.

One dimensional Ripa system with non-flat bottom

In this case, the bottom function $B(x)$ is assumed as a step-type. This step-type bottom is positioned at x_0, where the flow variables are initially discontinuous. The one-dimensional Ripa system with non-flat bottom topography has the following form [3]

$$\begin{aligned} &\partial_t h + \partial_x(hu) = 0,\\ &\partial_t hu + \partial_x\left(hu^2 + \tfrac{gh^2\theta}{2}\right) = -gh\theta\partial_x B,\\ &\partial_t h\theta + \partial_x(hu\theta) = 0,\\ &\partial_t B = 0. \end{aligned} \tag{37}$$

where h is the free surface elevation, $H = h + B$ is the total depth, $B = B(x)$ is the height of bottom from a given level, u is the x-

component of velocity, g is the acceleration due to gravity and $\theta > 0$ is the temperature of liquid.

The system (37) can be written as in compact form as

$$\frac{\partial w_i}{\partial t} + \frac{\partial f_i}{\partial x} = s_i, \quad i = 1,2,3,4, \tag{38}$$

where $w_1 \overset{\text{def}}{=} h$, $w_2 \overset{\text{def}}{=} hu$, $w_3 \overset{\text{def}}{=} h\theta$, $w_4 \overset{\text{def}}{=} B$, and the fluxes are given as

$$f_1 \overset{\text{def}}{=} w_2, \quad f_2 \overset{\text{def}}{=} \frac{(w_2)^2}{w_1} + \frac{g}{2}(w_1)(w_3), \quad f_3 \overset{\text{def}}{=} \frac{(w_2)(w_3)}{w_1}, \quad f_4 \overset{\text{def}}{=} 0. \tag{39}$$

Moreover,

$$s_1 = 0, \quad s_2 \overset{\text{def}}{=} -gw_3\frac{\partial B}{\partial x} \quad s_3 = 0 \quad s_4 = 0. \tag{40}$$

Eigenstructure for the Ripa system with non-flat bottom

The quasi-linear form of Ripa system is given as

$$\partial_t \mathbf{w} + A(\mathbf{w})\partial_x(\mathbf{w}) = 0, \tag{41}$$

where $\mathbf{w} = (w_1, w_2, w_3, w_4)^T$ and the Jacobian matrix $A(\mathbf{w})$ is defined as

$$A(\mathbf{w}) = \begin{pmatrix} 0 & 1 & 0 & 0 \\ -\frac{w_2^2}{w_1^2} + \frac{gw_3}{2} & 2\frac{w_2}{w_1} & \frac{gw_1}{2} & gw_3 \\ -\frac{w_2 w_3}{w_1^2} & \frac{w_3}{w_1} & \frac{w_2}{w_1} & 0 \\ 0 & 0 & 0 & 0 \end{pmatrix} = \begin{pmatrix} 0 & 1 & 0 & 0 \\ -u^2 + \frac{gh\theta}{2} & 2u & \frac{gh}{2} & gh\theta \\ -u\theta & \theta & u & 0 \\ 0 & 0 & 0 & 0 \end{pmatrix}. \tag{42}$$

The eigenvalues of the matrix A are expressed as

$$\lambda_1 = u - a, \lambda_2 = u, \lambda_3 = u + a, \lambda_4 = 0 \quad \textit{where} \quad a = \sqrt{gh\theta}$$

The corresponding eigenvectors are given by

$$\mathbf{r}_1 = \begin{pmatrix} 1 \\ u-a \\ \theta \\ 0 \end{pmatrix}, \quad \mathbf{r}_2 = \begin{pmatrix} 1 \\ u \\ -\theta \\ 0 \end{pmatrix}, \quad \mathbf{r}_3 = \begin{pmatrix} 1 \\ u+a \\ \theta \\ 0 \end{pmatrix}, \quad \mathbf{r}_4 = \begin{pmatrix} -a \\ 0 \\ -a\theta \\ u^2 - gh\theta \end{pmatrix}. \tag{43}$$

Lemma 1. *The first and fourth characteristic speeds and the third and fourth characteristic speeds can coincide on a hypersurface. Hence, the Ripa system becomes non-strictly hyperbolic.*

Here, we consider only strictly hyperbolic system which is only possible when $|u| \neq \sqrt{gh\theta}$.

Proposition 2. *The characteristic fields $\lambda_1(\mathbf{w})$ and $\lambda_3(\mathbf{w})$ are genuinely nonlinear fields and the characteristic fields $\lambda_2(\mathbf{w})$ and $\lambda_4(\mathbf{w})$ are linearly degenerate fields.*

Proof. As a first step, we prove that the characteristics fields $\lambda_1(\mathbf{w})$ and $\lambda_3(\mathbf{w})$ are genuinely nonlinear fields.

$$\begin{aligned} \nabla\lambda_1(\mathbf{w}) \cdot \mathbf{r}_1(\mathbf{w}) &= \left(\frac{-u}{h}, \frac{1}{h}, -0.5 * \sqrt{\frac{g}{h\theta}}, 0\right) \cdot (1, u-a, \theta, 0) \\ &= \frac{-a}{h} - 0.5 * \sqrt{\frac{g\theta}{h}} \neq 0, \end{aligned} \tag{44}$$

$$\begin{aligned} \nabla\lambda_3(\mathbf{w}) \cdot \mathbf{r}_3(\mathbf{w}) &= \left(\frac{-u}{h}, \frac{1}{h}, 0.5 * \sqrt{\frac{g}{h\theta}}, 0\right) \cdot (1, u+a, \theta, 0) \\ &= \frac{a}{h} + 0.5 * \sqrt{\frac{g\theta}{h}} \neq 0. \end{aligned} \tag{45}$$

Next, we prove that the characteristic fields $\lambda_2(\mathbf{w})$ and $\lambda_4(\mathbf{w})$ are linearly degenerate fields.

$$\nabla\lambda_3(\mathbf{w}) \cdot \mathbf{r}_3(\mathbf{w}) = \left(\frac{-u}{h}, \frac{1}{h}, 0, 0\right) \cdot (1, u, -\theta, 0) = 0,$$

$$\nabla\lambda_4(\mathbf{w}) \cdot \mathbf{r}_4(\mathbf{w}) = (0,0,0,0) \cdot (-a, 0, -a\theta, u^2 - \varphi\theta) = 0.$$

This completes the proof. □

Solution of the Ripa system with non-flat bottom

The structure of the solution of the Riemann problem consists of four waves, one for each eigenvalue $\lambda_i, i = 1,2,3,4$. The left most wave is either a shock wave or a rarefaction wave and, similarly, the right most wave is either a shock wave or a rarefaction wave depending on the given initial data. The third wave is called contact wave which always lies between shock wave and rarefaction waves. The fourth wave is called stationary shock wave located at x_0. These four waves make five different regions as shown in the Fig. 2, such as $w_L(h_L, u_L, \theta_L)$-left initial state, $w_R(h_R, u_R, \theta_R)$-right initial state, $w_{L*}(h_{L*}, u_{L*}, \theta_{L*})$-an unknown state left to the stationary shock wave, $w_{R*}(h_{R*}, u_{R*}, \theta_{R*})$-an unknown state right to the stationary shock wave, and $w_*(h_*, u_*, \theta_*)$-an unknown state right to the contact wave.

Rankine-Hugoniot relation for step bottom topography

By using the principles of mass, momentum and energy conservations, we can derive the Rankine-Hugoniot jump conditions across the stationary shock wave, for detail see [2]. Assume that single moving discontinuity connects the initial left and right states. We take flow region made up of water lying between two planes for the derivation of Rankine-Hugoniot conditions. Consider the x_R and x_L are the position of initial right and left planes and the single moving discontinuity is positioned at d. By dividing the integral in (51) into two parts at d, then taking the limit $x_L \to d$, $x_R \to d$, the Rankine-Hugoniot jump conditions for the Ripa system (37) becomes

$$-S[h] + [hu] = 0, \tag{46}$$

$$-S[hu] + [hu^2 + \frac{1}{2}gh^2\theta] = \beta, \tag{47}$$

$$-S[h\theta] + [h\theta u] = 0, \tag{48}$$

$$-S[B] = 0, \tag{49}$$

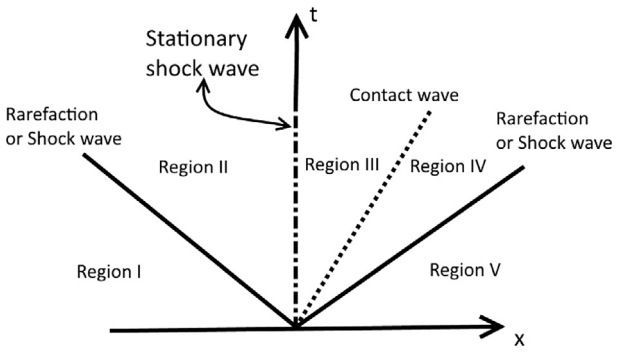

Fig. 2. Schematic diagram of five solution regions in the case of variable bottom.

where $[\cdot]$ denotes jump across the discontinuity. The term β, representing the force exerted on step-type bottom by fluid (with the minus sign) which is responsible for the bottom variation, is defined as

$$\begin{aligned}\beta = \int_{x_L}^{x_R} -g\theta h B_x dx &= \int_{x_L}^{x_R} -g\theta(H-B)B_x dx \\ &= \int_{x_L}^{x_R} -g\theta H B_x dx + \int_{x_L}^{x_R} g\theta B B_x dx \\ &= \int_{x_L}^{x_R} -g\theta H B_x dx + \int_{x_L}^{x_R} \tfrac{1}{2} g\theta B_x^2 dx \\ &= \left[-g\tfrac{(\theta_L H_L + \theta_R H_R)}{2}(B_R - B_L)\right] + \left[\tfrac{g}{2}\tfrac{(\theta_L+\theta_R)}{2}(B_R^2 - B_L^2)\right].\end{aligned} \tag{50}$$

From Lemma 3, $\theta_L = \theta_R$. Hence we can write

$$\begin{aligned}\beta &= \left[-g\theta_L \tfrac{(H_L+H_R)}{2}(B_R - B_L)\right] + \left[\tfrac{g\theta_L}{2}(B_R^2 - B_L^2)\right] \\ &= \tfrac{g\theta_L}{2}\left[-(H_L+H_R)(B_R - B_L) + (B_R^2 - B_L^2)\right] \\ &= \tfrac{g\theta_L}{2}(B_R - B_L)[-(H_L+H_R) + (B_R + B_L)] \\ &= \tfrac{g\theta_L}{2}(B_R - B_L)[-H_L + B_L - H_R + B_R)] \\ &= \tfrac{g\theta_L}{2}(B_R - B_L)[-h_L - h_R)] \\ &= \tfrac{g\theta_L}{2}(B_L - B_R)[h_L + h_R)].\end{aligned} \tag{51}$$

From Eq. (49) there are two possibilities [13].

(*i*) The bottom function $B(x)$ remains constant across the propagating discontinuity.

(*ii*) The bottom function $B(x)$ does not remain constant but the stationary shock wave has zero speed.

Firstly, assume that bottom function is constant. Then, Eqs. (46)–(49) become

$$-S[h] + [hu] = 0, \tag{52}$$

$$-S[hu] + [hu^2 + \frac{g}{2}h^2\theta] = 0, \tag{53}$$

$$-S[h\theta] + [h\theta u] = 0. \tag{54}$$

This case is similar as discussed in the previous section.

Secondly, assume that the bottom function $B(x)$ is not constant so that the speed S vanishes ($S = 0$). Then Eqs. (46)–(49) become

$$\begin{aligned}[hu] &= 0, \\ \left[hu^2 + \frac{g}{2}h^2\theta\right] &= \beta, \\ [h\theta u] &= 0.\end{aligned} \tag{55}$$

Hence, the stationary shock waves have zero speed and satisfy the Rankine-Hugoniot jump conditions in Eq. (55). The system in Eq. (55) can be rewritten as

$$\begin{aligned}h_{L*}u_{L*} &= h_{R*}u_{R*}, \\ h_{L*}u_{L*}^2 + \tfrac{g}{2}h_{L*}^2\theta_{L*} &= h_{R*}u_{R*}^2 + \tfrac{g}{2}h_{R*}^2\theta_{R*} + \beta, \\ h_{L*}\theta_{L*}u_{L*} &= h_{R*}\theta_{R*}u_{R*}.\end{aligned} \tag{56}$$

These conditions define a relation between the left and right states across a step-type bottom discontinuity. Also, these mass, momentum and energy conservation laws across the bottom step are satisfied by left and right columns of mass of water.

Properties of stationary shock waves

Lemma 3. *The temperature remains constant across the stationary shock wave.*

Proof. We can easily prove this lemma by using the first and third equations of system of Eqs. (55).

Suppose a state $w_L = (h_L, u_L, \theta_L, B_L)$ and $B \neq B_L$ are given, and the state on the other side of stationary shock wave is $w = (h, u, \theta, B)$ which is issued from a given state w_L. By putting $u = \frac{h_L u_L}{h}$ from the first equation of system of Eqs. (55) into the second equation of system of Eqs. (55), we obtain

$$\sigma(h) = -h_L u_L^2 - \frac{g}{2}h_L^2\theta_L + \frac{(h_L u_L)^2}{h} + \frac{g}{2}h^2\theta - \frac{g\theta_L}{2}(h_L + h)(B_L - B),$$

or by using Lemma 3, we get

$$\sigma(h) = -h_L u_L^2 - \frac{g}{2}h_L^2\theta_L + \frac{(h_L u_L)^2}{h} + \frac{g}{2}h^2\theta_L - \frac{g\theta_L}{2}(h_L + h)(B_L - B). \quad \square \tag{57}$$

Now, we analyze some useful properties of $\sigma(h)$.

Lemma 4. *Suppose a state $w_L = (h_L, u_L, \theta_L, B_L)$ and B are given with $u_L \neq 0$. The function $\sigma(h)$ is smooth and convex. Furthermore, the function $\sigma(h)$ is decreasing in the interval $(0, h_{min})$ and increasing in the interval (h_{min}, ∞) for $h > 0$, with*

$$\lim_{h\to 0}\sigma(h) = \lim_{h\to\infty}\sigma(h) = \infty.$$

Proof.

The smoothness of function is obvious and for the value of h_{min}, we differentiate Eq. (57) as

$$\frac{d\sigma(h)}{dh} = -\frac{(h_L u_L)^2}{h^2} + gh\theta_L - 0.5g\theta_L(B_L - B).$$

By setting

$$\frac{d\sigma(h)}{dh} = -\frac{(h_L u_L)^2}{h^2} + gh\theta_L - 0.5g\theta_L(B_L - B) = 0,$$

we have

$$h^3 - 0.5(B_L - B)h^2 - \frac{(h_L u_L)^2}{g\theta_L} = 0.$$

The last equation is of the form

$$x^3 + ax^2 + b = 0, \tag{58}$$

where $a = -0.5(B_L - B), b = -\frac{(h_L u_L)^2}{g\theta_L}$ and $x = h$. After solving Eq. (58), we get

$$\begin{aligned}\varphi_{min}(w_L) = &\left(\frac{-q}{2} + \sqrt[3]{\left(\frac{q}{2}\right)^2 + \left(\frac{p}{3}\right)^3}\right) \\ &- \left(\frac{q}{2} + \sqrt[3]{\left(\frac{q}{2}\right)^2 + \left(\frac{p}{3}\right)^3}\right) - \frac{a}{3},\end{aligned} \tag{59}$$

where $p = \frac{-a^2}{3}$ and $q = \frac{(2a^3+27b)}{27}$.

For $u_i \neq 0$ and $\varphi > 0, \frac{d\sigma(h)}{dh} > 0$if and only if $h > h_{min}(w_L)$. This means that the function $\sigma(h)$ is monotone. As $\theta_L > 0$ and $h > 0$, we have

$$\frac{d^2\sigma(h)}{dh^2} = 2\frac{(h_i u_L)^2}{h^3} + g\theta_L \geqslant 0.$$

In other words, the function $\sigma(h)$ is convex. $\square$

Corollary 1. *i) If $\sigma(h_{min}) < 0$ then the equation $\sigma(h) = 0$ has two roots, as shown in Fig. 3 (a). ii) If $\sigma(h_{min}) > 0$ then the equation $\sigma(h) = 0$ has no root, as shown in Fig. 3(b). iii) If $\sigma(h_{min}) = 0$ then the equation $\sigma(h) = 0$ has exactly one root.*

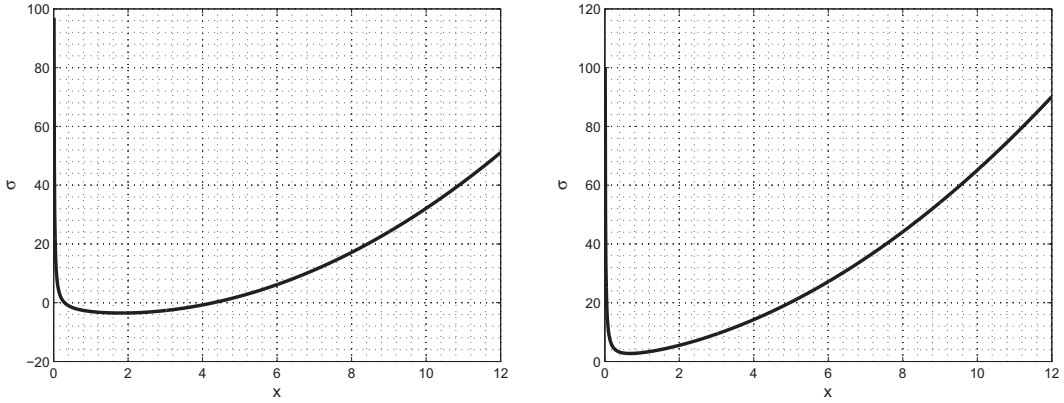

(a) The function σ has two roots. (b) The function σ has no root.

Fig. 3. For figure (a) $u_L = 1, h_L = 1, B_i = 3, B = 0, g = 1$ and for figure (b) $u_L = 1, h_L = 1, B_i = 0, B = 3, g = 1$.

Solution procedure

For the solution procedure of Ripa system with constant bottom, we take start at the contact discontinuity where $u_{L*} = u_{R*}$ and $h_{L*}^2\theta_L = h_{R*}^2\theta_R$. Therefore, by equating the equations

$$u_{L*} = \begin{cases} u_L - 2\sqrt{g\theta_L}(\sqrt{h_{L*}} - \sqrt{h_L}) & h_{L*} < h_L, \\ u_L - (h_{L*} - h_L)\sqrt{\frac{g\theta_L}{2}\frac{(h_L + h_{L*})}{h_L h_{L*}}} & h_{L*} > h_L, \end{cases} \tag{60}$$

and

$$u_{R*} = \begin{cases} u_R + 2\sqrt{g\theta_R}(\sqrt{h_{R*}} - \sqrt{h_R}) & h_{R*} < h_R, \\ u_R + (h_{R*} - h_R)\sqrt{\frac{g\theta_R}{2}\frac{(h_R + h_{R*})}{h_R h_{R*}}} & h_{R*} > h_R, \end{cases} \tag{61}$$

we get a nonlinear equation with two unknowns h_{L*} and h_{R*}. We put the value of $h_{L*} = h_{R*}\sqrt{\frac{\theta_R}{\theta_L}}$ in that nonlinear equation and solve the resulting equation iteratively for the value of h_{R*}. Once the nonlinear equation is solved, we continue our solution procedure in a conventional manner, see [14] for more detail. Usually this nonlinear equation is solved by using the Newton–Raphson iterative method

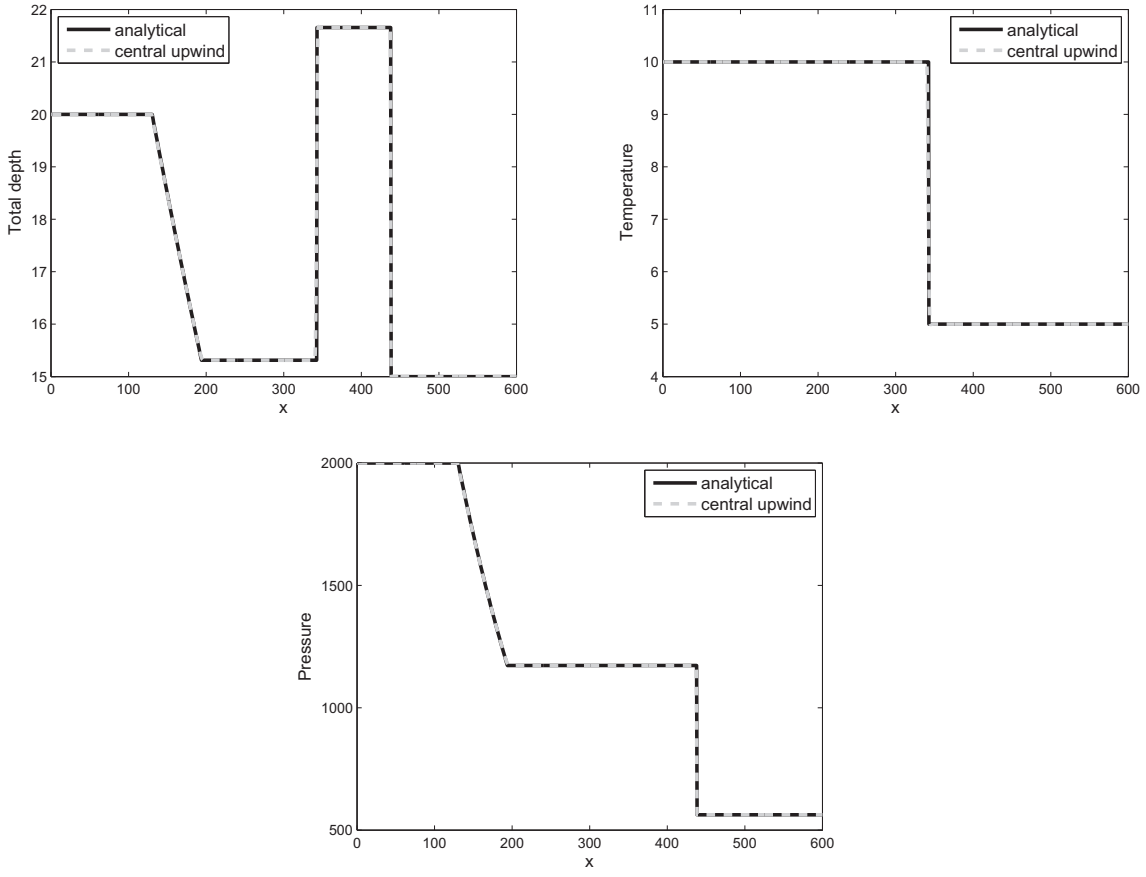

Fig. 4. H, θ, and p are computed by the proposed exact Riemann solver and by central upwind scheme at = 12.

and an initial guess $h_{R*}^{(0)}$ for this iterative procedure is taken as $h_{R*}^{(0)} = \frac{1}{2}(a_L^2 + a_R^2)$, or two rarefaction approximation as $h_{R*}^{(0)} = \frac{1}{g}\left(\frac{1}{2}(a_L + a_R) + \frac{1}{4}(u_R - u_L)\right)^2$, for more detail see [20]. For the solution of Ripa system with non-flat bottom, we use the Eqs. (60) and (61) in the Eq. (56) and solve the resulting system of algebraic equations for h_{L*} and h_{R*}. After obtaining the values of h_{L*} and h_{R*} we complete our solution procedure in the same way as done for the case of constant bottom topography. In this article, both the nonlinear equation and system of nonlinear equations are solved by using the MATLAB function "*fsolve*".

Numerical tests

This section presents several numerical case studies for the Ripa system with constant and variable bottom topographies. For verification, the analytical results are compared with the numerical results of central upwind scheme obtained in a computational domain $[0, 600]$. In all case studies, the computational domain is divided into 2400 grid points for the numerical scheme, the value of gravity $g = 1$ and the bottom step is positioned at $x = 300$ with height 3 to the right of the origin. To elaborate each solution of given examples, we sketch the state wave diagram

$$\mathbf{w}_1 \xrightarrow{\text{RW}} \mathbf{w}_2 \xrightarrow{\text{SSW}} \mathbf{w}_3 \xrightarrow{\text{CW}} \mathbf{w}_4 \xrightarrow{\text{SW}} \mathbf{w}_5,$$

which tells us that the given initial left state $\mathbf{w}_1$ is connected with state $\mathbf{w}_2$ by a rarefaction wave 'RW' and the state $\mathbf{w}_2$ is connected with the state $\mathbf{w}_3$ by a stationary shock wave 'SSW' and the state $\mathbf{w}_3$ is connected with the state $\mathbf{w}_4$ by a contact wave 'CW', and the state $\mathbf{w}_4$ is connected with the state $\mathbf{w}_5$ by a shock wave 'SW'.

Test Problem 1: Consider the dam break problem over a flat bottom with the following initial conditions

$$(H, u, \theta)(x, 0) = \begin{cases} (20, 0, 10), & x \le 300, \\ (15, 0, 5), & x > 300. \end{cases}$$

In Fig. 4, the exact and approximate solutions are plotted in the computational domain $[0, 600]$ at time $= 12$ for the total depth H, the pressure $p = \frac{g\varphi^2\theta}{2}$ and the temperature θ. The state wave diagram for the solution is given as

$$\mathbf{w}_1 \xrightarrow{\text{RW}} \mathbf{w}_2 \xrightarrow{\text{CW}} \mathbf{w}_3 \xrightarrow{\text{SW}} \mathbf{w}_4.$$

Good agreements among analytical and numerical results verify the correctness of analytical solutions and accuracy of the proposed numerical algorithm.

Test Problem 2: Next, we consider the dam break problem over a discontinuous bottom topography for the following initial conditions:

$$(H, u, \theta, B)(x, 0) = \begin{cases} (20, 0, 10, 0), & x \le 300, \\ (15, 0, 5, 3), & x > 300. \end{cases}$$

The state wave diagram for the solution is expressed as

$$\mathbf{w}_1 \xrightarrow{\text{RW}} \mathbf{w}_2 \xrightarrow{\text{SSW}} \mathbf{w}_3 \xrightarrow{\text{CW}} \mathbf{w}_4 \xrightarrow{\text{SW}} \mathbf{w}_5,$$

The analytical and numerical solutions are presented in Fig. 5. Both analytical and numerical results agree with each other.

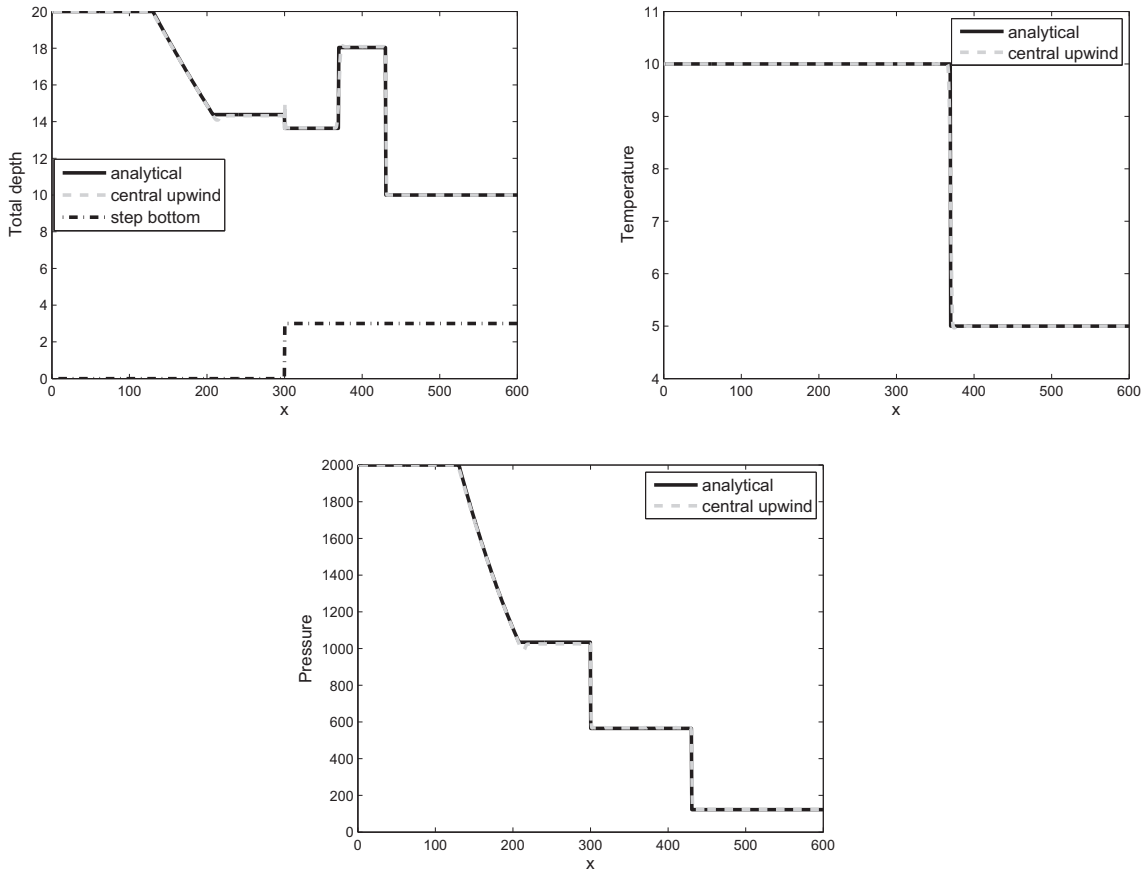

Fig. 5. H, θ, and p are computed by the proposed exact Riemann solver and by central upwind scheme at $= 12$.

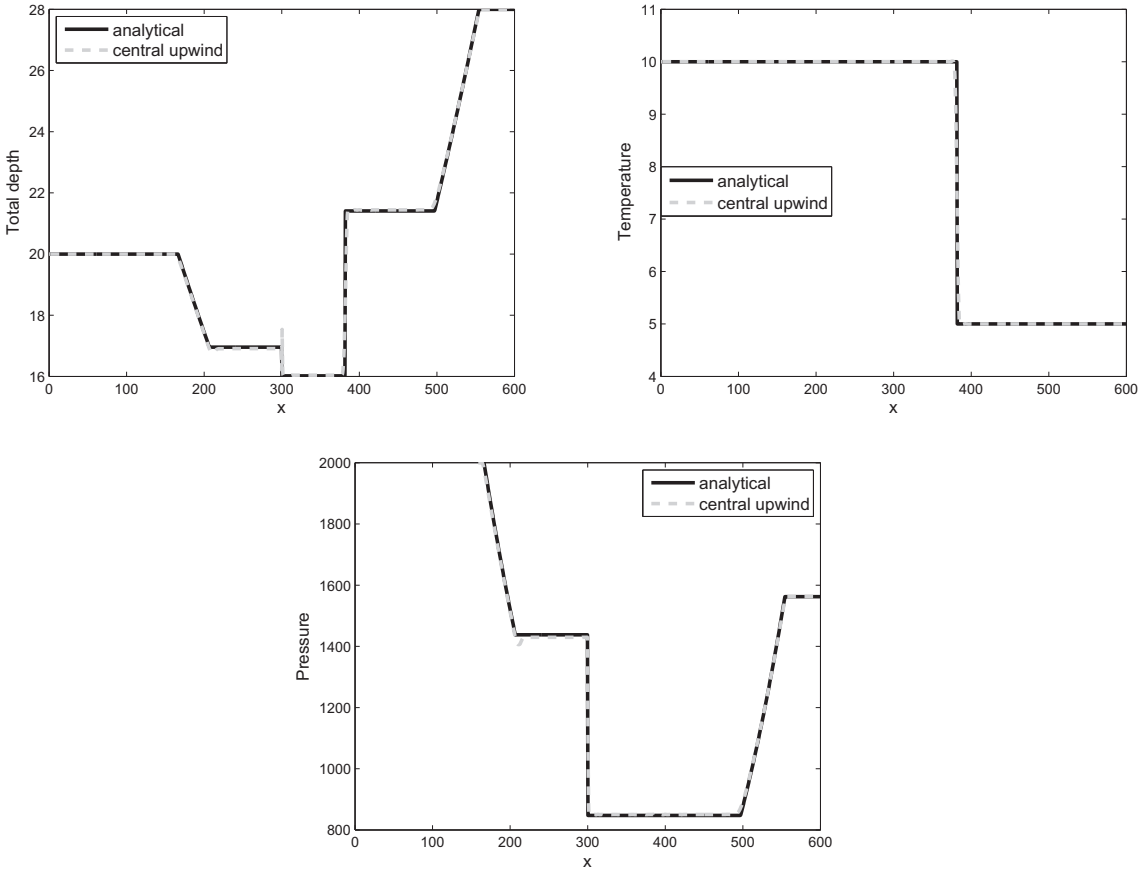

Fig. 6. H, θ, and p are computed by the suggested exact Riemann solver and by central upwind scheme at time = 12.

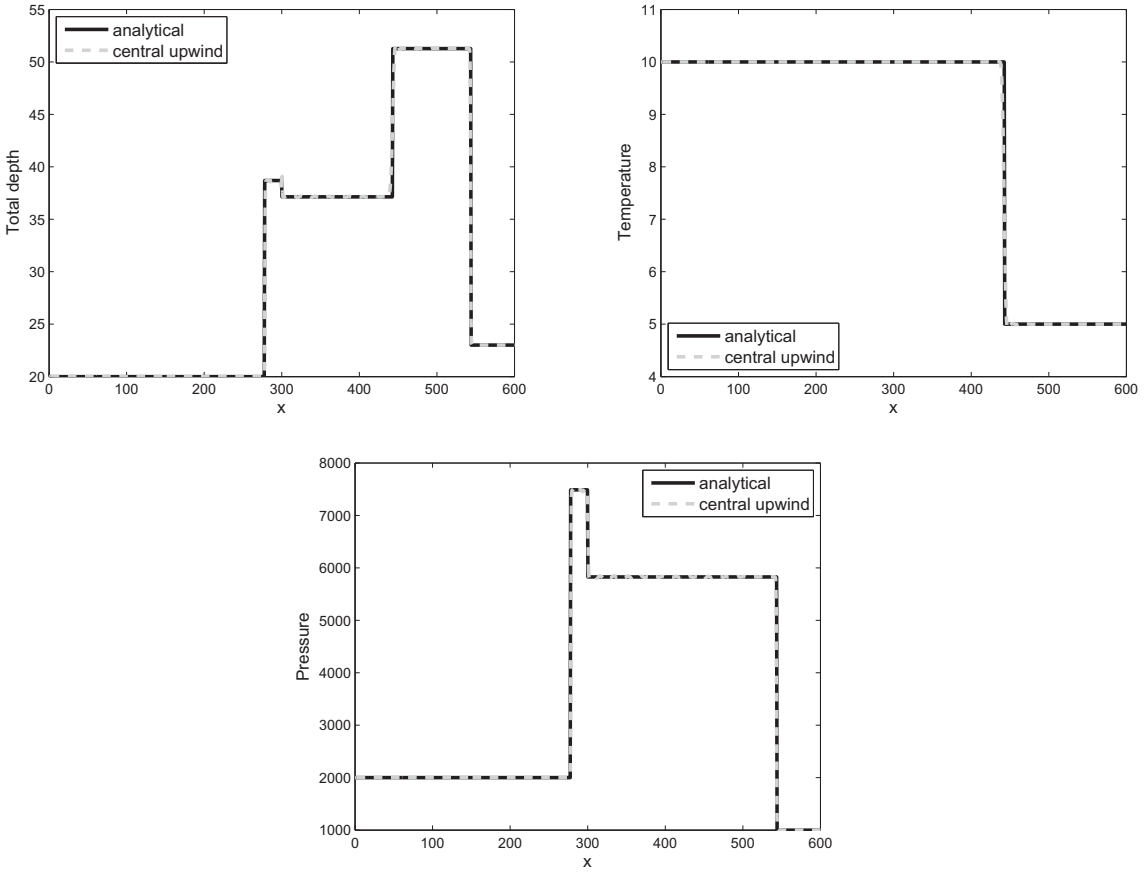

Fig. 7. H, θ, and p are computed by the suggested exact Riemann solver and by central upwind scheme at time = 12.

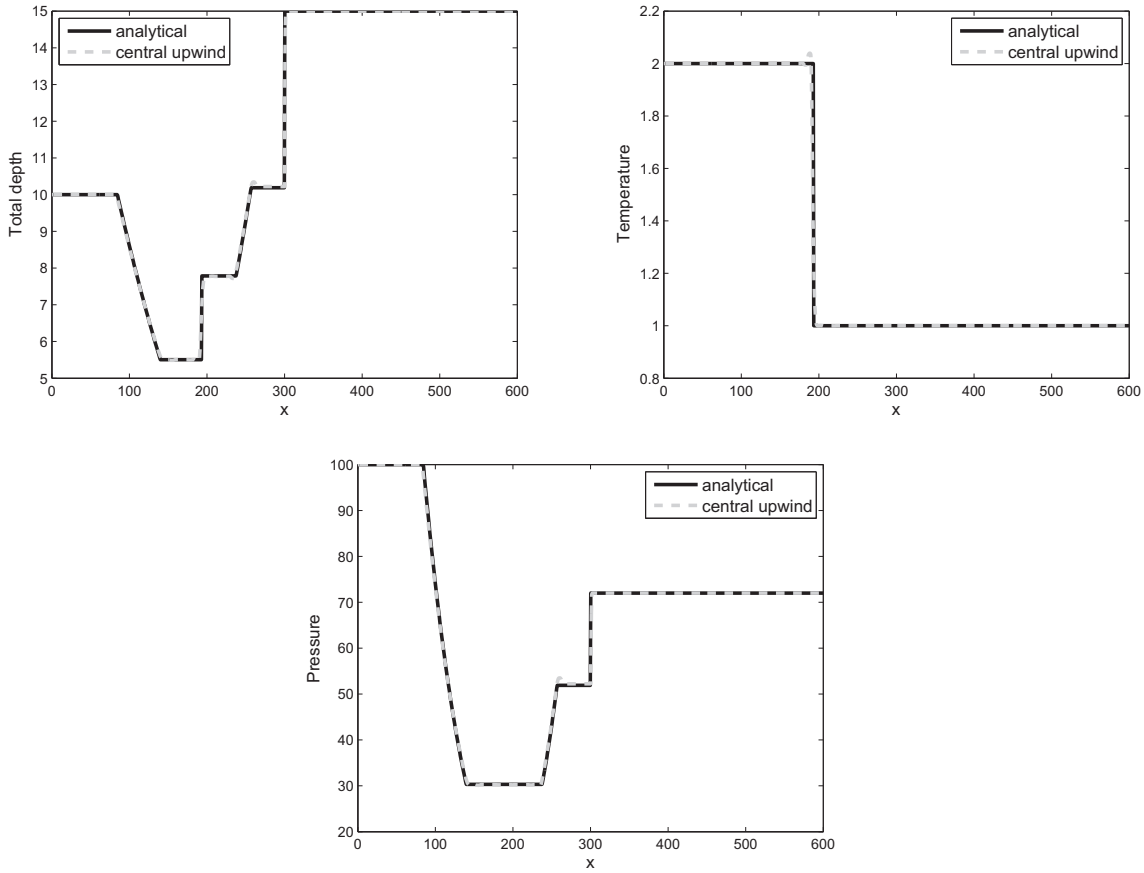

Fig. 8. H, θ, and p are computed by the suggested exact Riemann solver and by central upwind scheme at time = 16.

Test Problem 3: Consider the problem of discontinuous bottom topography which is subjected to the following initial conditions:

$$(H,u,\theta,B)(x,0) = \begin{cases} (20,3,10,0), & x \leq 300, \\ (25,10,5,3), & x > 300. \end{cases}$$

The solution is presented in Fig. 6 and the state wave diagram for the solution takes the form

$$\mathbf{w}_1 \xrightarrow{\text{RW}} \mathbf{w}_2 \xrightarrow{\text{SSW}} \mathbf{w}_3 \xrightarrow{\text{CW}} \mathbf{w}_4 \xrightarrow{\text{RW}} \mathbf{w}_5.$$

Both analytical numerical results show a good agreement with each other.

Test Problem 4: Consider the problem of discontinuous bottom topography with the following initial conditions

$$(H,u,\theta,B)(x,0) = \begin{cases} (20,22,10,0), & x \leqslant 300 \\ (20,0,5,3), & x > 300. \end{cases}$$

In this example the state wave diagram takes the form

$$\mathbf{w}_1 \xrightarrow{\text{CW}} \mathbf{w}_2 \xrightarrow{\text{SSW}} \mathbf{w}_3 \xrightarrow{\text{CW}} \mathbf{w}_4 \xrightarrow{\text{SW}} \mathbf{w}_5,$$

and solution is presented in Fig. 7. Excellent agreement can be seen in analytical and numerical results.

Test Problem 5: The initial conditions for such type of a problem are

$$(H,u,\theta,B)(x,0) = \begin{cases} (10,-9,2,0), & x < 300 \\ (12,-5,1,3), & x > 300. \end{cases}$$

The state wave diagram for the solution is

$$\mathbf{w}_1 \xrightarrow{\text{RW}} \mathbf{w}_2 \xrightarrow{\text{CW}} \mathbf{w}_3 \xrightarrow{\text{RW}} \mathbf{w}_4 \xrightarrow{\text{SSW}} \mathbf{w}_5 = \mathbf{w}_6.$$

In this example, the flow is from right to left and two rarefaction waves are pushed to the left as shown in the Fig. 8. The solution is obtained at $t = 16$. Once again, both analytical and numerical solutions agree well with each other.

Test Problem 6: This is a test problem of discontinuous bottom topography in which two shocks are pushed to the right of the step as shown in the Fig. 9. The system is subjected to the following initial conditions:

$$(H,u,\theta,B)(x,0) = \begin{cases} (12,16,2,0), & x < 300 \\ (4,2,8,3), & x > 300. \end{cases}$$

In this example, the state wave diagram takes the following form

$$\mathbf{w}_1 = \mathbf{w}_2 \xrightarrow{\text{SSW}} \mathbf{w}_3 \xrightarrow{\text{SW}} \mathbf{w}_4 \xrightarrow{\text{CW}} \mathbf{w}_5 \xrightarrow{\text{SW}} \mathbf{w}_6.$$

Once more time, both analytical and numerical solutions agree well with each other.

Conclusions

The analytical Riemann solutions of the Ripa model for flat and non-flat bottom topographies are presented. In the case of non-flat bottom topography, the Rankine-Hugoniot jump conditions across the step-type bottom were derived by employing the mass, momentum and energy conservation laws. The analytical results

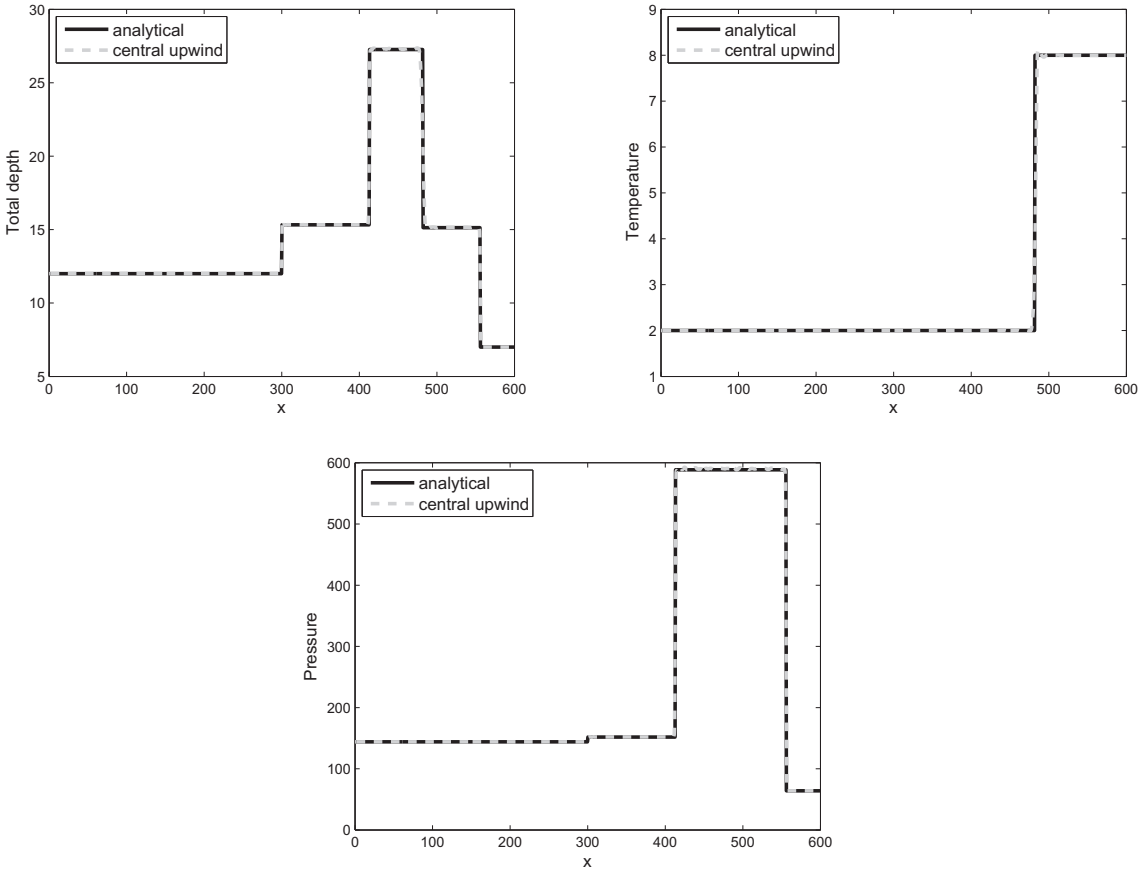

Fig. 9. H, θ, and p are computed by the suggested exact Riemann solver and by central upwind scheme at time = 16.

are compared with numerical solutions of high resolution central scheme. A good agreement was found between the solutions of both types of solvers.

Acknowledgement

The second author is thankful to the support of Marie Currie Alumni Association.

References

[1] Alcrudo F, Benkhaldoun F. Exact solutions to the Riemann problem of the shallow water equations with a bottom step. Comput Fluids 2001;30:643–71.
[2] Bernetti R, Titarev VA, Toro EF. Exact solution of the Riemann problem for the shallow water equations with discontinuous bottom geometry. J Comput Phys 2008;227:3212–43.
[3] Chertock A, Kurganov A, Liu Y. Central-Upwind schemes for the system of shallow water equations with horizontal temperature gradients. Numerische Math 2013;127:595–639.
[4] Dellar PJ. Common Hamiltonian structure of the shallow water equations with horizontal temperature gradients and magnetic fields. Phys Fluids 2003;15:292–7.
[5] Desveaux V, Zenk M, Berthon C, Klingenberg C. Well-Balanced schemes to capture non-Explicit steady states: Ripa model. Math Comput 2016;85:1571–602.
[6] Gosse L. A well-Balanced flux-Vector splitting scheme designed for hyperbolic systems of conservation laws with source terms. Comput Math Appl 2000;39:135–59.
[7] Greenberg JM, Leroux AY. A Well-Balanced Scheme for the Numerical Processing of Source Terms in Hyperbolic Equations. SIAM J Numer Anal 1996;33:1–16.
[8] Han E, Warnecke G. The exact Riemann solutions to Shallow-water equations. Appl Math 2012.
[9] Han X, Li G. Well-Balanced finite difference WENO schemes for the Ripa model. Comput Fluids 2016:134–5.
[10] Jin S, Wen X. Two interface-type numerical methods for computing hyperbolic systems with geometrical source terms having concentrations. SIAM J Sci Comput 2005;26:2079–101.
[11] Karelsky KV, Papkov VV, Petrosyan AS, Tsygankov DV. Particular solutions of shallow-water equations over a non-flat surface. Phys Lett A 2000;271:341–8.
[12] Krner D, Thanh MD. Numerical Solutions to Compressible Flows in a Nozzle with Variable Cross-Section. SIAM J Numer Anal 2005;43:796–824.
[13] Lefloch PG, Thanh MD. The riemann problem for fluid flows in a nozzle with discontinuous cross-section. Commun Math Sci 2003;1:763–97.
[14] LeVeque RJ. Finite Volume Methods for Hyperbolic Problems. Cambridge: Cambridge Univ. Press; 2011.
[15] Nessyahu H, Tadmor E. Non-Oscillatory central differencing for hyperbolic conservation laws. J Comput Phys 1990;87:408–63.
[16] Ripa P. Conservation laws for primitive equations models with inhomogeneous layers. Geophys Astrophys Fluid Dyn 1993;70:85–111.
[17] Ripa P. On improving a one-Layer ocean model with thermodynamics. J Fluid Mech 1995;303:169–201.
[18] Snchez-Linares C, De Luna TM, Castro Daz MJ. A HLLC scheme for Ripa model, Applied. Math Comput 2016;272:369–84.
[19] Szydleowski M. Implicit versus explicit finite volume schemes for extreme, free surface water flow modeling. Arch Hydroeng Env Mech 2004;51:287–303.
[20] Toro EF. Riemann solvers and numerical methods for fluid dynamics a practical introduction. Berlin Heidelberg: Springer; 2009.
[21] Wen X. A steady state capturing and preserving method for computing hyperbolic systems with geometrical source terms having concentrations. J Comput Phys 2006;219:322–90.